Protein Crystals

DOI: 10.1002/anie.201001043

Microemulsion-Mediated Self-Assembly and Silicification of Mesostructured Ferritin Nanocrystals**

*Elizabeth M. Lambert, Chulanapa Viravaidya, Mei Li, and Stephen Mann**

Nanoscale objects with advanced structure and function are of considerable interest in areas such as sensing, drug delivery and bioelectronics,[1,2] and have important implications for biotoxicity[3,4] and the emergence of life.[5] In many cases, the synthesis and structuration of hybrid nano-objects is achieved under equilibrium or non-equilibrium conditions through a range of strategies involving integrative, higher-order, or transformative self-assembly.[6,7] Often these approaches involve the confinement and templating of reactions on or within supramolecular assemblies such as dendrimers,[8] organogel nanofilaments,[9] peptide fibers,[10] helical micelles,[11] virus capsids,[12] and protein cages.[13] Recently, cross-linked lysozyme crystals, approximately 200 μm in size, have been used to prepare nanoplasmonic arrays by intracrystalline metallization,[14] suggesting that the high mesoporosity of protein crystals might be exploited in general for the template-directed assembly of organized inorganic nanostructures across a range of length scales. Whilst many common proteins readily form crystals with macroscopic dimensions, it is generally difficult to produce nanoscale counterparts that would be effective as templates for the preparation of discrete hybrid nanomaterials. In this regard, the iron storage protein, ferritin, which consists of a 12 nm diameter spherical polypeptide shell enclosing a 5–6 nm sized iron oxide core[15] is known to readily form two-dimensional (2D) superlattices on various substrates[16] and can be clustered into aggregates in solution using biotin–streptavidin linkages or inorganic nanoparticles.[17] It should therefore be possible to control the self-assembly of discrete nanometer-sized ferritin crystals, and as a consequence use these nanocrystals as porous templates for the fabrication of hybrid nanoparticles with ordered mesostructured interiors.

Here, we use water-in-oil microemulsion droplets as a medium for controlling the aggregation of entrapped ferritin molecules to produce discrete protein nanocrystals that can be stabilized by in situ silicification of the intracrystalline voids to produce mesostructured silica–ferritin hybrids. Microemulsions are versatile reaction media for the confinement and synthesis of inorganic nanoparticles,[18] nanowires,[19] nanoparticle superlattices,[20] and complex hierarchical architectures.[21] In addition, microemulsion droplets have been used for the encapsulation of drugs,[22] exploration of organic chemical reactions,[23] entrapment of functional enzymes,[24] and for the separation of protein mixtures.[25] Although droplet instability can often be a problem in these applications, herein we demonstrate that protein-mediated aggregation of the water pools can be exploited to produce discrete ferritin nanocrystals and silicified counterparts with well-ordered close packed structures. As silicification of the interstitial pores occurs with high precision and without degradation of the protein, it should be possible to extend our approach to a wide range of biomimetic ferritins as well as to other globular proteins and synthetic analogues such as metal-encapsulated dendrimers.

Addition of aqueous ferritin (Fn) to 0.1 M sodium bis(2-ethylhexyl)sulfosuccinate (NaAOT)/isooctane solutions at water to surfactant molar ratios (w) of 20 or 45 and ferritin concentrations of 45 or 15 μM, respectively, resulted in homogeneous orange-colored water-in-oil microemulsions. Samples prepared at 31 °C were stable with respect to bulk sedimentation for at least 24 h, whilst those at 4 °C produced an orange precipitate within 2 h. Dynamic light scattering (DLS) measurements indicated that inclusion of the protein in the surfactant-stabilized water pools resulted in a significant increase in droplet size when compared to the protein-free microemulsions prepared at the same w values. In the absence of ferritin, the DLS profiles for microemulsions prepared at $w = 45$ or 20 showed single peaks corresponding to monodisperse distributions of water droplets of mean diameter 24 or 10 nm, respectively (Supporting Information, Figure S1), which did not change in size over a period of 3 h. Significantly, the droplet size determined at $w = 20$ was less than the diameter of the ferritin molecule (12 nm). In contrast, in the presence of ferritin and at $w = 45$ ([Fn] = 15 μM; P = number ratio of initial water droplets to ferritin molecules = 85), a bimodal distribution of droplet sizes centred initially at 18 and 120 nm was observed (Figure S1a). Under these conditions the droplets were mainly within the smaller size range, which remained essentially unchanged with time, whilst the larger droplets showed a progressive increase in diameter to give a relatively broad distribution with a mean value of 460 nm after 2 h. These results were consistent with slow coalescence of the primary droplets due to increases in the instability of the nanoscale water pools in the presence of encapsulated ferritin molecules. In comparison, at $w = 20$ ([Fn] = 45 μM, $P = 324$), protein sequestration in the water droplets immediately gave rise to aggregates with a mean diameter of 615 nm that did not substantially undergo

[*] E. M. Lambert, Dr. C. Viravaidya, Dr. M. Li, Prof. S. Mann
Centre for Organized Matter Chemistry
School of Chemistry, University of Bristol
Bristol, BS8 1TS (UK)
E-mail: s.mann@bristol.ac.uk
Homepage: http://www.chm.bris.ac.uk/inorg/mann/webpage.htm

[**] This work was supported by the EPSRC (UK). We thank D. S. Williams for help with DLS studies and Dr. S. A. Davis for assistance with TEM analysis.

Supporting information for this article is available on the WWW under http://dx.doi.org/10.1002/anie.201001043.

further aggregation (Figure S1b). Thus, the rate of droplet coalescence was significantly increased at $w = 20$ compared with $w = 45$. We attributed this to the increased instability of the microemulsion interface when the initial droplet size was commensurate with that of the ferritin guest molecules.

TEM studies of the ferritin-containing microemulsions prepared as above and investigated within similar time domains revealed that droplet coalescence was associated with localized self-assembly of the ferritin molecules. TEM images of samples extracted up to 24 h after microemulsion preparation at $w = 20$ showed the presence of large numbers of spheroidal particles many of which comprised a 3D mesoordered array of close packed ferritin molecules, typically between 40 and 550 nm in size (mean = 200 nm) (Figure 1 a,b). Similar studies on ferritin-containing microemulsions prepared at $w = 45$ also revealed mesostructured ferritin nanocrystals (Figure 1 c) but the yields were significantly lower than at $w = 20$ particularly for relatively short incubation periods. Unfiltered and filtered fast Fourier transforms (FFT) of the TEM images (Figure S2) revealed that the ferritin nanocrystals had a cubic close-packed structure (a = 21.6 nm), which consisted of {111} planes of ferritin molecules spaced at an intermolecular distance of 12.3 nm. EDX analysis of the ferritin nanocrystals showed the presence of Fe and P from the iron oxide/phosphate cores of the protein, as well as S from the protein and/or NaAOT surfactant (Figure 1 d). The presence of surfactant molecules in the ferritin nanocrystals was confirmed from values of the normalized Fe:S peak intensity ratios that were significantly lower compared with those determined from the EDX spectra of native ferritin (typical values; 3:1 and 6:1, respectively; Figure S3).

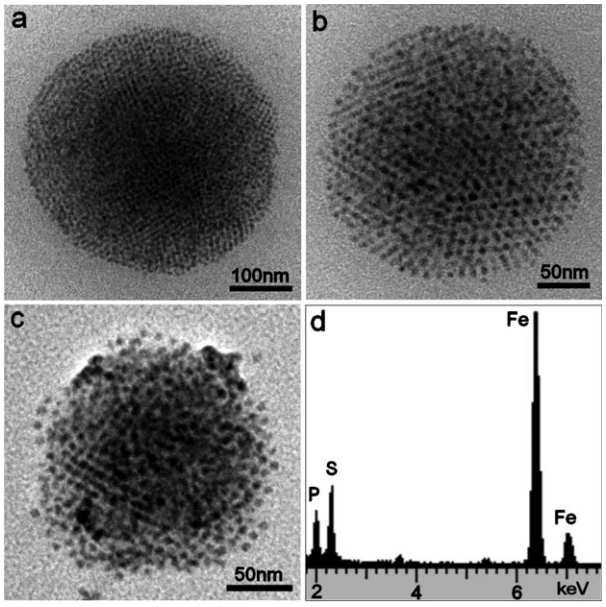

Figure 1. TEM images of ferritin nanocrystals prepared in NaAOT microemulsions and showing periodically ordered 3D mesostructured arrays. a,b) $w = 20$, $P = 700$, $T = 4\,°C$, $t = 8.5$ h (a) and 24 h (b). c) Sample prepared at $w = 45$, [Fn] = 15 μM, $P = 85$, $T = 31\,°C$, $t = 5.5$ h. In each case, the electron dense dots correspond to the 5 nm sized iron oxide cores of ferritin. d) EDX analysis of an individual ferritin nanocrystal showing peaks for P, S, and Fe. Trace peaks at 3.7 and 5.4 keV (Ca and Cr, respectively) are from contamination and the sample holder.

In situ silicification of the ferritin nanocrystals was achieved by undertaking similar experiments but with tetramethoxysilane (TMOS) dissolved in the oil phase of the microemulsion. In general, low rates of silicification and relatively high protein concentrations ([Fn] = 45 μM) were required for high fidelity replication of the intracrystalline spaces. At $w = 20$ and 31 °C, this was established by using a H value (H = water:silica molar ratio) of 150, a TMOS:ferritin molar ratio of 8000:1, and a high number of initial water droplets per protein molecule ($P = 324$) to stabilize the high ferritin concentration. (Corresponding values used at $w = 20$ and 4 °C were [Fn] = 48 μM, $P = 253$, $H = 150$, TMOS:protein = 7700:1). Under these optimum conditions, addition of TMOS to homogeneous ferritin-containing microemulsions prepared at $w = 20$ produced an orange precipitate after 2–5 h, which could be washed and isolated as a solid powder after 24 h (Figure 2 a). TGA studies typically gave a ferritin content of around 20 wt % (Figure S4). SEM images of the powders revealed discrete particles of variable size that were clearly mineralized; for example, at 4 °C, the particles were 0.5–2.5 μm (mean 1.3 μm ($\sigma = 0.6$)) in diameter with a roughened surface texture and occasionally were partially collapsed under the vacuum, suggesting a relatively soft microstructure (Figure 2 b). TEM images showed the presence of a large number of spheroidal mesostructured particles

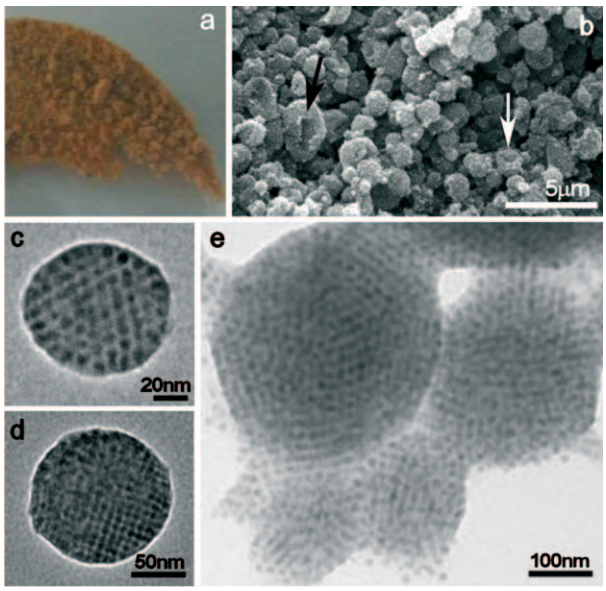

Figure 2. Silica–ferritin nanocrystals prepared in NaAOT microemulsions at $w = 20$. a) Optical photograph showing bulk powder produced after air-drying; b) SEM image showing discrete spheroidal silica–ferritin particles. Arrows highlight partially collapsed particles. c–e) TEM images of discrete silica–ferritin nanocrystals with mesoordered interiors; samples prepared at c,d) $T = 4\,°C$, $t = 2$ h and e) $T = 31\,°C$, $t = 2$ h.

comprising self-assembled ordered arrays of protein molecules encased within a continuous matrix of amorphous silica (Figure 2c–e). The particle diameters varied from approximately 100 nm to around 0.5 μm with a mean value of 200 nm ($\sigma = 90$) (Figure S5). In contrast, control experiments involving the addition of TMOS to protein-free NaAOT reverse microemulsions at $w = 20$, $H = 150$ and $T = 4$ or 31 °C, produced monodisperse non-structured spheroidal silica nanoparticles with mean sizes of 13.7 nm ($\sigma = 3$) or 16 nm ($\sigma = 3$), respectively (Figure S6). In both cases, the silica nanoparticles were significantly smaller than the mesostructured silica–ferritin nanocrystals, indicating that droplet coalescence was not significantly induced by TMOS alone.

Measurement of the lattice spacings and FFT analysis of the silica–ferritin nanocrystals were consistent with retention of the cubic close-packed structure after silicification (Figure S7). Diffraction patterns of the hybrid nanocrystals viewed along the [111] or [001] zones were indexed to a cubic unit cell of length $a = 20.8$ nm, which was slightly reduced compared with the lattice parameter (21.3 nm) determined prior to addition of TMOS to the microemulsions. The absence of an expanded lattice parameter suggested that silica deposition was confined specifically to the interstitial void spaces, such as octahedral and tetrahedral holes in the nanocrystal structure, which for a close-packed ferritin array were calculated to be 2.8 and 5.1 nm in size, respectively.

Interestingly, it was possible to reductively dissolve the iron oxide cores of the silica–ferritin hybrid nanoparticles without significant disruption of the particle size or internal cubic close-packed mesostructure (Figure 3a), indicating that

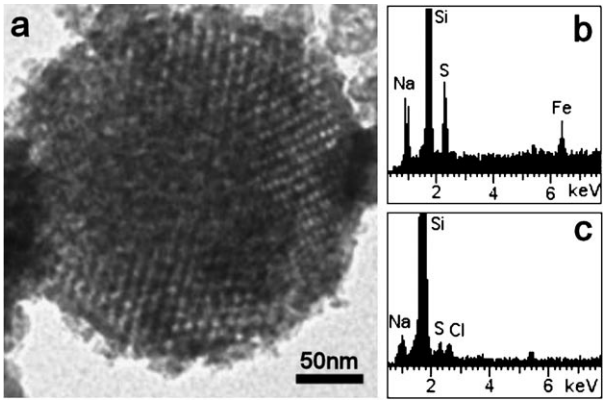

Figure 3. a) TEM image of hybrid nanocrystal after in situ removal of the iron oxide cores of ferritin. The white dots correspond to the empty cavities of apoferritin molecules organized within the silica matrix. b,c) EDX spectra for silica–ferritin nanocrystals before (b) and after (c) iron core demineralization.

the protein cavity remained accessible to small molecules such as thioglycolic acid when entrapped within the inorganic matrix. This was confirmed by EDX analysis of the as-prepared or demineralized hybrid nanoparticles, which showed peaks for Si (1.7 keV), S (2.3 keV) and Fe (6.4 keV), or Si and S, respectively (Figure 3b,c). Moreover, FTIR spectra of these samples showed silica absorption bands at 1100, 960, 800, and 470 cm^{-1}, as well as amide I (C=O/C–N str) and amide II peaks (N–H bends/C–H str) at around 1650 and 1550 cm^{-1}, respectively, confirming that the encapsulated protein molecules retained their native α-helical secondary structure both during silicification and after in situ demineralization of the iron oxide cores (Figure S8). The FT-IR spectra also indicated that AOT but not ferritin molecules could be extracted from the silica–ferritin nanoparticles by extensive washing (Figure S8).

Brunauer–Emmett–Teller (BET) nitrogen adsorption–desorption measurements indicated that the silica–ferritin nanocrystals showed type IV mesoporosity with low surface areas, which increased from 60 $m^2 g^{-1}$ for the as-prepared hybrid nanocrystals to 89 $m^2 g^{-1}$ after in situ demineralization (Figure S9a,b). Removal of the protein molecules by thermal treatment at 350 °C for 1 h (TGA studies) increased the surface area to 260 $m^2 g^{-1}$ (Figure S9c,d) with retention of type IV mesoporosity. This was confirmed by XRD studies that showed broadened low-angle reflections at 12.6, 7.4, and 5.5 nm corresponding to the {111}, {220}, and {400} of a poorly ordered cubic close packed mesostructure (Figure S10).

In general, formation of well-ordered silica–ferritin nanocrystals was favored under conditions in which the protein self-assembly was faster than silicification. At low [TMOS] this was facilitated by relatively high protein concentrations and the increased instability of the ferritin/NaAOT microemulsions produced at $w = 20$, which together induced rapid droplet coalescence. As a consequence, the protein molecules self-assembled into ordered arrays prior to patterned silica deposition within the interstitial spaces of the ferritin nanocrystal. This process was facilitated at relatively low temperatures; indeed raising the temperature to 60 °C gave only disordered arrays of ferritin molecules entrapped within networks of irregularly shaped silicified particles. In contrast, silicification reactions undertaken for up to 24 h in ferritin/NaAOT microemulsions prepared at $w = 45$ or 50 ($H = 100$, [Fn] = 15 or 7.8 μM, respectively), in which droplet aggregation was considerably slower, produced high yields of silica nanoparticles comprising isolated protein molecules (Figure 4a). Typically, the silica particles were 40 nm ($\sigma = 6$) in mean size, and in general contained between one and six (mean = three) protein molecules per particle (Figure 4b). Demineralization studies indicated that the iron cores of the entrapped protein molecules could be chemically removed to produce silica nanoparticles comprising isolated spherical voids associated with intact polypeptide shells of apoferritin (Figure 4c). Larger aggregates were less commonly observed and, where present, appeared to contain ferritin molecules randomly dispersed within the particles.

In conclusion, the spontaneous self-assembly of well-ordered ferritin cubic close-packed nanocrystals with average particle sizes around 200 nm was facilitated by enforced coalescence of protein-containing microemulsion water droplets at a w value of 20. Under these conditions, the initial droplet size was commensurate with the dimension of the ferritin guest molecules, and as a consequence the host–guest environment transforms rapidly to produce ordered 3D arrays of hydrophobic surfactant-coated protein molecules encapsulated within the expanded water pools. Addition of

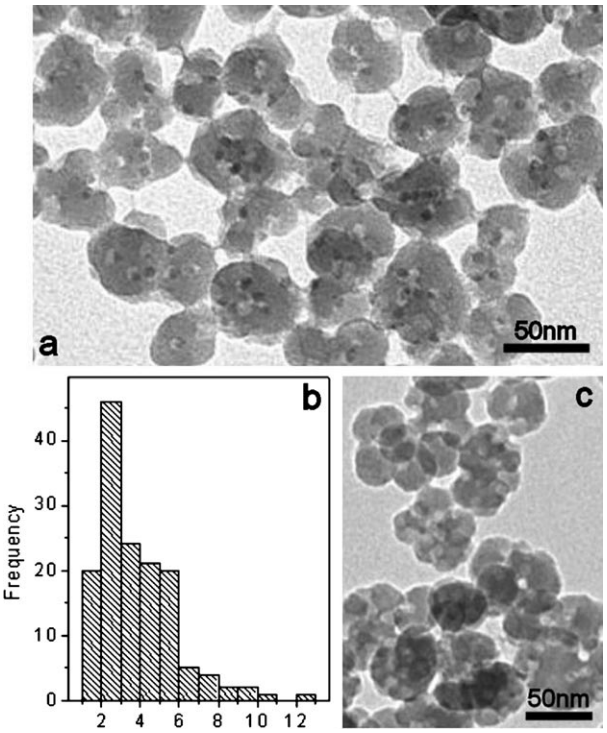

Figure 4. Formation of isolated ferritin molecules in silica nanoparticles prepared in NaAOT microemulsions at $w = 50$, $T = 31\,^{\circ}C$, [Fn] = 7.8 μM, $P = 120$, $H = 100$. a) TEM image showing encapsulation of discrete ferritin molecules. b) Distribution of number of entrapped ferritin molecules per silica nanoparticle. c) TEM image of particles after in situ demineralization of the iron oxide cores.

TMOS to these microemulsions under conditions in which nanocrystal assembly is faster than the hydrolysis/condensation kinetics of silicification, results in efficient infilling of the interstitial nanospaces of the protein array with amorphous silica. The inorganic matrix remains sufficiently porous and hydrated to allow in situ reductive dissolution of the embedded ferritin iron oxide cores to produce a hybrid mesostructure consisting of a cubic close-packed array of protein nanocages. In contrast, reducing droplet instability by using microemulsions prepared at $w = 45$ gave isolated or small clusters of ferritin molecules encapsulated within discrete silica nanoparticles. Finally, as the methods described are facile, it should be possible to exploit microemulsion-mediated self-assembly to prepare diverse types of mesostructured protein-based nanocrystals for applications in areas such as catalysis, storage and release, sensing, and nanoplasmonics.

Experimental Section

Methods for the preparation and silicification of ferritin nanocrystals, preparation of ordered silica–ferritin mesostructured nanocrystals, iron oxide core demineralization in silica–ferritin nanocrystals, and entrapment of isolated ferritin molecules in silica nanoparticles are described in the Supporting Information.

Received: February 19, 2010
Revised: March 22, 2010
Published online: April 28, 2010

Keywords: ferritin · mesostructures · protein crystals · self-assembly · silica

[1] C. A. Mirkin, C. M. Niemeyer, *Nanobiotechnology II*, Wiley-VCH, Weinheim, **2007**.
[2] E. Katz, I. Willner, *Angew. Chem.* **2004**, *116*, 6166; *Angew. Chem. Int. Ed.* **2004**, *43*, 6042.
[3] A. Nel, T. Xia, L. Madler, N. Li, *Science* **2006**, *311*, 622.
[4] G. Bhabra, A. Sood, B. Fisher, L. Cartwright, M. Saunders, W. H. Evans, A. Surprenant, G. Lopez-Castejon, S. Mann, S. A. Davis, L. A. Hails, E. Ingham, P. Verkade, J. Lane, K. Heesom, R. Newson, C. P. Case, *Nat. Nanotechnol.* **2009**, *4*, 876.
[5] S. Mann, *Angew. Chem.* **2008**, *120*, 5386; *Angew. Chem. Int. Ed.* **2008**, *47*, 5306.
[6] X. Wang, J. Zhuang, Q. Peng, Y. D. Li, *Nature* **2005**, *437*, 121.
[7] S. Mann, *Nat. Mater.* **2009**, *8*, 781.
[8] B. I. Lemon, R. M. Crooks, *J. Am. Chem. Soc.* **2000**, *122*, 12886.
[9] K. J. C. van Bommel, A. Friggeri, S. Shinkai, *Angew. Chem.* **2003**, *115*, 1010; *Angew. Chem. Int. Ed.* **2003**, *42*, 980.
[10] J. D. Hartgerink, E. Beniash, S. I. Stupp, *Science* **2001**, *294*, 1684.
[11] E. D. Sone, E. R. Zubarev, S. I. Stupp, *Small* **2005**, *1*, 694.
[12] S. E. Aniagyei, C. DuFort, C. C. Kao, B. Dragnea, *J. Mater. Chem.* **2008**, *18*, 3763.
[13] M. Li, C. Viravaidya, S. Mann, *Small* **2007**, *3*, 1477.
[14] M. Guli, E. M. Lambert, M. Li, S. Mann, *Angew. Chem.* **2010**, *122*, 530; *Angew. Chem. Int. Ed.* **2010**, *49*, 520.
[15] E. C. Theil, *Annu. Rev. Biochem.* **1987**, *56*, 289.
[16] a) M. Yamaki, K. Matsubara, K. Nagayama, *Langmuir* **1993**, *9*, 3154; b) M. Matsumoto, *Langmuir* **1994**, *10*, 3922.
[17] a) M. Li, K. K. W. Wong, S. Mann, *Chem. Mater.* **1999**, *11*, 23; b) S. Srivastava, B. Samanta, B. J. Jordan, R. Hong, Q. Xiao, M. T. Tuominen, V. M. Rotello, *J. Am. Chem. Soc.* **2007**, *129*, 11776.
[18] a) Y. H. Jin, S. Lohstreter, D. T. Pierce, J. Parisien, M. Wu, C. Hall III, J. X. J. Zhao, *Chem. Mater.* **2008**, *20*, 4411; b) K. Naoe, C. Petit, M. P. Pileni, *Langmuir* **2008**, *24*, 2792; c) S. Vaucher, M. Li, S. Mann, *Angew. Chem.* **2000**, *112*, 1863; *Angew. Chem. Int. Ed.* **2000**, *39*, 1793.
[19] a) Y. Xing, M. Li, S. A. Davis, S. Mann, *J. Phys. Chem. B* **2006**, *110*, 1111; b) M. P. Pileni, T. Gulik-Krzywicki, J. Tanori, A. Filankembo, J. C. Dedieu, *Langmuir* **1998**, *14*, 7359.
[20] a) M. Li, H. Schnablegger, S. Mann, *Nature* **1999**, *402*, 393; b) C. J. Johnson, M. Li, S. Mann, *Adv. Funct. Mater.* **2004**, *14*, 1233; c) T. Isojima, S. K. Suh, J. B. V. Sande, T. A. Hatton, *Langmuir* **2009**, *25*, 8292.
[21] a) H. Cölfen, S. Mann, *Angew. Chem.* **2003**, *115*, 2452; *Angew. Chem. Int. Ed.* **2003**, *42*, 2350; b) M. Li, S. Mann, *Langmuir* **2000**, *16*, 7088; c) M. Li, S. Mann, *Adv. Funct. Mater.* **2002**, *12*, 773; d) M. Li, B. Lebeau, S. Mann, *Adv. Mater.* **2003**, *15*, 2032.
[22] S. Gupta, S. P. Moulik, *J. Pharm. Sci.* **2008**, *97*, 22.
[23] a) F. Michel, M. P. Pileni, *Langmuir* **1994**, *10*, 390; b) N. M. Correa, E. N. Durantini, J. J. Silber, *J. Phys. Org. Chem.* **2006**, *19*, 805.
[24] N. I. Gerhardt, S. R. Dungan, *Biotechnol. Bioeng.* **2002**, *78*, 60.
[25] L. H. Poppenborg, A. A. Brillis, D. C. Stuckey, *Sep. Sci. Technol.* **2000**, *35*, 843.

